Fault gouge graphitization as evidence of past seismic slip

Li-Wei Kuo[1]*, Fabio Di Felice[2], Elena Spagnuolo[2], Giulio Di Toro[2,3,4], Sheng-Rong Song[5], Stefano Aretusini[3], Haibing Li[6], John Suppe[7], Jialiang Si[6], and Cheng-Yen Wen[8]

[1]*Department of Earth Sciences, National Central University, Taoyuan 320, Taiwan*

[2]*Istituto Nazionale di Geofisica e Vulcanologia, 00143 Rome, Italy*

[3]*School of Earth and Environmental Sciences, University of Manchester, Manchester M13 9PL, UK*

[4] *Department of Geosciences, Università di Padova, 35122 Padua, Italy*

[5]*Department of Geosciences, National Taiwan University, Taipei 106, Taiwan*

[6] *Chinese Academy of Geological Sciences, 100037 Beijing, China*

[7]*Department of Earth and Atmospheric Science, University of Houston, Houston, Texas 77004, USA*

[8] *Department of Material Science and Engineering, National Taiwan University, Taipei 106, Taiwan*

*E-mail: liweikuo@ncu.edu.tw

ABSTRACT

One moderate- to large-magnitude earthquake (M > 6) nucleates in Earth's crust every three days, but the geological record of ancient fault slip at m/s seismic velocities (as opposed to subseismic slow-slip creep) remains debated because of the lack of established fault-zone evidence of seismic slip. Here we show that the irreversible temperature-dependent transformation of carbonaceous materials (CMs, a constituent of many fault gouges) into graphite is a reliable tracer of seismic fault slip. We sheared

CMs-bearing fault rocks in the laboratory at almost subseismic and at seismic velocities under both water-rich and -deficient conditions and modeled the temperature evolution with slip. By means of micro-Raman spectroscopy and focused-ion beam transmission electron microscopy, we detected graphite grains similar to those found in the principal slip zone of the 2009 Wenchuan (M_w 7.9) earthquake only in experiments conducted at seismic velocities. The experimental evidence presented here suggests that high temperatures pulses associated to seismic slip induce graphitization of CMs. Importantly, the occurrence of graphitized fault-zone CMs may allow us to ascertain the seismogenic potential of faults in areas worldwide with incomplete historical earthquake catalogues.

INTRODUCTION

Fault rocks accommodate the most of slip during earthquakes (Sibson, 2003), but their record of deformation events occurring at typical seismic slip rates of ~1m/s, as opposed to slow-slip and aseismic creep events, remains uncertain because of the lack of univocal characteristics (Cowan, 1999; Rowe and Griffith, 2015). Seismic slip is thought to be accommodated in centimeter- to submillimeter-thick slipping zones, and localized frictional sliding may trigger processes such as flash heating and melting, dehydration and decarbonation reactions, and thermal decomposition of fault rocks (Sibson, 2003; Di Toro et al., 2011). Because of the relatively high seismic slip rates at seismogenic depths, natural slipping zone should record abrupt and transient increase in temperature during earthquakes. Importantly, disordered organic compounds or amorphous carbonaceous materials (CMs) can be progressively and irreversibly transformed into stable graphite through thermally activated graphitization (Buseck and Beyssac, 2014). Therefore, the progressive increase in crystallographic order of CMs associated with graphitization is

widely utilized as indicators of the maximum temperatures achieved by sedimentary and metamorphic rocks (Barker and Goldstein, 1990; Beyssac et al., 2002). Because CMs are also found in natural fault zones, its graphitization may provide valuable information on earthquake mechanics (Oohashi et al., 2012).

Fault-zone graphitization has been proposed for the principal slip zone (PSZ) of the Longmenshan thrust fault that ruptured in a devastating 2008 M_w 7.9 Wenchuan earthquake in southeast Tibet (Kuo et al., 2014). According to the Wenchuan earthquake Fault Scientific Drilling-1 (WFSD-1) data, at 590 m depth, the active fault zone includes an ~54-cm-thick black gouge made of quartz, feldspar, clay minerals plus graphite and CMs, surrounded by an ~2-m-thick fault breccia made of quartz, feldspar, calcite, clay minerals, CMs (mainly poorly crystalline anthracite), but without graphite (Fig. 1; Li et al., 2013; Si et al., 2014). Wang et al. (2014) demonstrated that CMs within the Wenchuan fault zone originated from adjacent host rocks (late Triassic Xujiahe Formation). Kuo et al. (2014) speculated that gouge graphitization occurred within CMs-bearing fault gouges during the 2008 M_w 7.9 Wenchuan earthquake. However, it remained unclear the process responsible for CMs graphitization, under which ambient and deformation conditions it occurred and, more relevant, if CMs graphitization could be only associated to seismic slip. These crucial questions are addressed here, where we also demonstrate that the experimental products obtained at seismic slip rates are almost identical to those found in the PSZ of the Longmenshan fault, making the CMs graphitization a powerful tool to investigate the seismogenic potential of active faults, especially if outcropping in areas with incomplete historical earthquake catalogues.

EXPERIMENTAL METHODS

To investigate the graphitization process of the CMs-bearing materials, we sheared with the rotary-shear machine SHIVA (Di Toro et al., 2010; Niemeijer et al., 2011) the graphite-free rocks of the fault breccia retrieved from 589.32 m depth. The bulk fault breccia were gently pulverized down to <250 μm in size and poured into a ring-shaped metal sample holder designed for confinement of non-cohesive materials (Smith et al., 2012). The gouges were sheared for 3 m of slip at equivalent slip rates, *V*, of 0.0003 m/s (simulating almost subseismic) and 3 m/s (seismic) slip rates under a normal stress of 8.5 MPa. The experiments were conducted on 5 g of gouges (corresponding to an initial thickness of ~3 mm) at room temperature and humidity and, by adding 0.5 g of distilled water, water-damped conditions. Deformed samples were collected for microanalytical investigations including micro-Raman spectroscopy, field-emission scanning electron microscopy (FESEM), and focused ion beam–transmission electron microscopy (FIB-TEM) equipped with an energy dispersive X-ray spectroscopy (EDS). The natural materials of the active fault zone (black gouge and breccia) were investigated with micro-Raman spectroscopy and compared with the experimental products (Fig. 1).

RESULTS

The mechanical data, consistent with previous studies (Oohashi et al., 2011; Rutter et al., 2013; Kuo et al., 2014; Kouketsu et al., 2017), resulted in two slip-velocity–dependent behaviors (Fig. 2; Item DR2 in the GSA Data Repository[1]). When sheared at seismic slip rates (V = 3 m/s), the experimental gouges showed pronounced weakening, with the apparent friction coefficient (defined as shear stress/normal stress) decaying, in the room-humidity experiments, from a peak value of 0.50 to a minimum value of 0.20, and in the water-damped experiments, from 0.18 to 0.02 (the latter had a quite

93 complicated evolution of the friction coefficient, with minimum friction followed by re-
94 strengthening up to 0.2 after 0.5 m and 0.25 after 2.3 m of slip). Instead, when the gouges
95 were sheared at almost subseismic slip rates (V = 0.0003 m/s), the effective friction
96 coefficient evolved with slip from an initial value of 0.40 up to ~0.55 under room-
97 humidity conditions, and from 0.26 to 0.37 under water-dampened conditions. The
98 temperature evolution with slip was modeled with COMSOL (https://www.comsol.com)
99 multiphysics using the measured frictional power dissipation (product of shear stress with
100 slip rate), and the thermal properties of the WFSD fault gouge (Item DR3; Li et al.,
101 2015). The initial temperature for the modeling was set to 25 °C. In the slipping zone of
102 the gouge layer sheared under room-humidity conditions at 3 m/s (s1108; seismic, RH in
103 Fig. 2), the modeled temperature rose from 25 °C to ~200 °C after 0.5 m of slip, and
104 further increased up to ~300 °C at the end of the experiment. Instead, under water-
105 dampened conditions (s1105; seismic, WD in Fig. 2), the temperature increased up to ~50
106 °C after 0.5 m of slip and progressively to ~280 °C till the sample was decelerated and
107 the experiment completed. The modeled temperature in the gouges sheared at almost
108 subseismic slip rates (V = 0.0003 m/s) was ~26 °C independent of the presence of liquid
109 water (Fig. 2).
110 In Raman spectroscopy, the peak parameters of the D1 (defect) band and the G
111 (graphite) band is commonly used as a gauge to quantify the degree of the graphitization
112 process (Beyssac et al., 2002; 2003) (Fig. 1b, inset; Item DR4). Here the ratio of D1 to G
113 peak width was compared with the ratio of D1 to G peak intensity. The ratio of D1 to G
114 peak width of either starting material (i.e., gouges) or fault breccia, normalized with the
115 average peak width of the fault breccia, was compared to peak position (i.e., Raman

shift). We analyzed five fault breccia samples, seven black gouge samples (including the PSZ of the 2009 Wenchuan earthquake), one starting material (fault breccia) and four experimental products; the latter obtained under a range of deformation conditions (Items DR5 and DR6).

The black gouge samples, compared to the fault breccia, have a lower D1/G peak intensity ratio and higher D1/G peak width ratio (Fig. 1b). Although fault breccia and black gouge have similar D1 band position, the G band position of the black gouge has higher frequency (Fig. 1c). In addition, the G peak width ratio of the black gouge was smaller than the one of the fault breccia.

Independent of the imposed slip rates and the presence of liquid water, the sheared gouges have a lower D1/G peak intensity ratio and higher D1/G peak width ratio, with respect to the starting materials (Fig. 3a). Both starting materials and deformed gouges have a similar D1 band position and peak width ratio (Fig. 3b). Variations occur in the G band position and peak width ratio, comparing sheared samples with starting material (Fig. 3b). In the sheared materials, the G band position is shifted to higher wavelength numbers independent of slip rates.

Strain localization in the gouge layers occurred during rock deformation experiments at both almost subseismic and seismic rates in both wet and room-humidity conditions, developing an experimental PSZ (Figs. 4a and 4b). Volumes of the slipping zones that underwent the highest degree of strain localization were investigated with FIB-TEM-EDS and selected area electron diffraction (SAED). Starting materials and gouges sheared at subseismic slip rates had amorphous carbon (i.e., no graphite) and similar random-range ordered regions of ~1–200 nm in size (Fig. 4c). On the contrary, gouges

sheared at seismic slip rates had perfectly stacking layers (lattice spacing of d002 ~3.55Å) in defect-free carbon-built grains with ordered structures, suggesting that amorphous carbon was transformed into graphitic carbon (Fig. 4d; Item DR1).

DISCUSSION AND CONCLUSION

Amorphous CMs usually contain two types of electronic configuration of carbon atoms: sp^3 or diamond-like, and sp^2 or graphite-like. The conversion of sp^3-bond into sp^2-bond results in graphitization of CMs and in the transformation of the latter into graphite (Ferrari and Robertson, 2000). It is well established that the D1/G peak intensity ratio is inversely proportional to the average size of the sp^2 clusters from conversion of sp^3 bonds (Fig. 3a; Ferrari and Robertson, 2000). In addition, the G band shifts toward higher frequencies in both the gouges sheared at subseismic and seismic slip rates (Fig. 3b). Therefore, the Raman spectra on experimental products shows that the transformation of sp^3-bond carbon into sp^2-bond carbon in the amorphous carbon network was driven by bulk shear strain, suggesting rehybridization of interacting dangling bonds of carbon during both subseismic and seismic slip (Pastewka et al., 2011).

Heating has been suggested to order phase of sp^2 and result in the formation of graphite from clusters of carbon atoms (Thomas et al., 2006), determining a smaller G band peak width (Beyssac et al., 2002). In the experiments performed on gouges at seismic slip rates and room-humidity conditions, high temperatures (up to 300 °C) were achieved during frictional sliding, and the small width ratio of G bands (red triangles in Figure 3b; Fig. 4d) suggest the crystallization of carbon into graphite. By contrast, in the water-dampened experiments performed on gouges at seismic slip rates, water vaporization possibly buffered the temperature increase (limited to <200 °C) and

impeded the formation of graphite (blue triangles in Figure 3b; Chen et al., 2017). Moreover, in the experiments performed at subseismic slip rates and independent of the water content, the temperature remained at to ~26 °C (Fig. 2). In the latter sheared gouges, the similar width ratio of both D1 and G compared to the starting materials suggest the presence of a random-order sp^2-bond domain (Figs. 3b and 4c; Item DR1) and, therefore, the absence of graphitization processes.

Our rock friction experiments demonstrate that CMs graphitization is characterized by (1) decreasing D/G peak intensity ratio, (2) shift of G peak position toward higher frequencies, and (3) smaller peak width ratio than the starting materials. The changes in the Raman spectra result from the formation of sp^2 clusters in the CMs due to strain (Ross and Bustin, 1990) rather than strain rate. Instead, the decrease in G band peak width ratio which indicates increased crystallinity of the CMs is attributed to frictional heating. As a consequence, the microstructural/mineralogical evolution of CMs (amorphous at almost subseismic slip rates and reordering and graphitization at seismic slip rates) may allow us to individuate active seismogenic faults. However, the absence of evidence of graphitization processes in CMs-bearing gouges (see wet experiments at seismic rates) is not indicative of the aseismic behavior of the faults.

Because our experiments at seismic slip rates, and in the absence of liquid water, showed enhanced graphitization of CMs (Fig. 3), we may interpret the analyses on WFSD-1fault rocks as follows. The anti-correlation between peak width ratio and peak intensity ratio suggests that the transformation of sp^3-bond carbon into sp^2-bond carbon occurs within the black gouge (Fig. 1b), and a shift to high frequency of G band from breccia to gouge is presumably due to strain (Fig. 1c). In particular, the narrower G peak

width of black gouge suggests that CMs contain abundant well-ordered sp^2 domains, implying that the black gouge was exposed to an increase in temperature under water-deficient conditions (Kuo et al., 2014). Permeability measurements of the WFSD-1 suggested that coseismic drainage was critical for later healing the fault damage associated to seismic rupture propagation (Xue et al., 2013). It seems likely that, during seismic slip, pore fluids were expelled from the slipping zone and seismic slip resulting in locally dry conditions allowing gouge graphitization. This hypothesis is consistent with the finding of pseudotachylytes (solidified friction melts typically associated to seismic slip under water-deficient conditions; Sibson and Toy, 2006) in the PSZ of the 2008 M_w 7.9 Wenchuan earthquake retrieved at ~1000 m depth from the WFSD-1 drill hole (Wang et al., 2016). In addition, because water circulation was vigorous within the fault zone following the main shock (Xue et al., 2013), other chemical interactions with carbon and hydrothermal fluid at various ambient conditions must be taken into consideration (Oohashi et al., 2012; Rumble, 2014).

Importantly, the fault-zone wall rocks have lower thermal conductivity (~1 $Wm^{-1}K^{-1}$) compared to the sample metal holder (~40 $Wm^{-1}K^{-1}$; Item DR3). In nature, compared to the experiments, this should result in a higher temperature rise and longer time duration of higher temperatures, favoring graphitization kinetics during seismic slip (Yao et al., 2015). However, the higher G peak width ratio of the natural gouges with respect to the gouge deformed at room-humidity conditions implies that the natural gouges were exposed to lower frictional power dissipation with respect to the experimental gouges. Coseismic fluid drainage (and water vaporization) efficiently dissipated the frictional heat generated during seismic slip, buffering the temperature

increase, and therefore resulting in smaller temperature-induced graphitization (Fig. 1c). The micro-Raman measurements presented here are in accordance with those from the WFSD-1 (Kuo et al., 2014; Si et al., 2014; Li et al., 2015) and agree that the Longmenshan fault was extremely weak during seismic slip.

Our results find application to determine seismic fault movement in general. Due to the resistance of graphitized products to alteration and weathering, the state of graphitization of CMs (if graphite is related to faulting and not due to precipitation from percolating fluids, etc.) could be a suitable indicator of historical or ancient earthquakes in faults. Only low-grade amorphous CMs were found in the surface rupture of the Longmenshan fault (Kouketsu et al., 2017), suggesting that gouge graphitization requires a certain amount of energy (shear stress, strain, and temperature) to be triggered (Kuo et al., 2014). As a consequence, the presence of graphite at depth (>500 m) within active fault zones might be a robust indicator of seismic hazard in areas worldwide with incomplete historical earthquake catalogues.

ACKNOWLEDGMENTS

This research used materials provided by the "Wenchuan earthquake Fault Scientific Drilling" program of the National Science and Technology Planning Project. We thank John Platt and two anonymous reviewers for their positive and constructive comments, and editor Dennis Brown for his help throughout the publication process. Part of this work was supported by the National Science Foundation of China (41330211, 41520104006) to Haibing Li, the European Research Council Consolidator Starting Grant 614705 NOFEAR to Giulio Di Toro, and Taiwan ROC (Republic of China) Ministry of

Science and Technology (MOST 105–2628-M-008–002-MY3) and NCU grants to Li-Wei Kuo.

REFERENCES CITED

Barker, C.E., and Goldstein, R.H., 1990, Fluid-inclusion technique for determining maximum temperature in calcite and its comparison to the vitrinite reflectance geothermometer: Geology, v. 18, p. 1003–1006, doi:10.1130/0091-7613(1990)018<1003:FITFDM>2.3.CO;2.

Beyssac, Q., Goffé, B., Chopin, C., and Rouzaud, J.N., 2002, Raman spectra of carbonaceous material in metasediments: A new geothermometer: Journal of Metamorphic Geology, v. 20, p. 859–871, doi:10.1046/j.1525-1314.2002.00408.x.

Beyssac, Q., Goffé, B., Petitet, J.P., Froigneux, E., Moreau, M., and Rouzaud, J.N., 2003, On the characterization of disordered and heterogeneous carbonaceous materials by Raman spectroscopy: Spectrochimica Acta Part A, v. 59, p. 2267–2276, doi:10.1016/S1386-1425(03)00070-2.

Buseck, P.R., and Beyssac, O., 2014, From organic matter to graphite: Graphitization: Elements, v. 10, p. 421–426, doi:10.2113/gselements.10.6.421.

Chen, J., Niemeijer, A., Yao, L., and Ma, S., 2017, Water vaporization promotes coseismic fluid pressurization and buffers temperature rise: Geophysical Research Letters, v. 44, p. 2177–2185.

Cowan, D.S., 1999, Do faults preserve a record of seismic slip? A field geologist's opinion: Journal of Structural Geology, v. 21, p. 995–1001, doi:10.1016/S0191-8141(99)00046-2.

252 Di Toro, G., et al., 2010, From field geology to earthquake simulation: A new state-of-
253 the-art tool to investigate rock friction during the seismic cycle (SHIVA): Rendiconti
254 Lincei. Scienze Fisiche e Naturali, v. 21, p. 95–114, doi:10.1007/s12210-010-0097-
255 x.
256 Di Toro, G., Han, R., Hirose, T., De Paola, N., Nielsen, S., Mizoguchi, K., Ferri, F.,
257 Cocco, M., and Shimamoto, T., 2011, Fault lubrication during earthquakes: Nature,
258 v. 471, p. 494–498, doi:10.1038/nature09838.
259 Ferrari, A.C., and Robertson, J., 2000, Interpretation of Raman spectra of disordered and
260 amorphous carbon: Physical Review B: Condensed Matter and Materials Physics,
261 v. 61, p. 14095–14107, doi:10.1103/PhysRevB.61.14095.
262 Kouketsu, Y., Shimizu, I., Wang, Y., Yao, L., Ma, S., and Shimamoto, T., 2017, Raman
263 spectra of carbonaceous materials in a fault zone in the Longmenshan thrust belt,
264 China; comparisonswith those of sedimentary and metamorphic rocks:
265 Tectonophysics, v. 699, p. 129–145, doi:10.1016/j.tecto.2017.01.015.
266 Kuo, L.W., Li, H., Smith, S., Di Toro, G., Suppe, J., Song, S.R., Nielsen, S., Sheu, H.S.,
267 and Si, J., 2014, Gouge graphitization and dynamic fault weakening during the 2008
268 Mw 7.9 Wenchuan earthquake: Geology, v. 42, p. 47–50, doi:10.1130/G34862.1.
269 Li, H., et al., 2013, Characteristics of the fault-related rocks, fault zones and the principal
270 slip zone in the Wenchuan earthquake Fault Scientific Drilling Hole-1 (WFSD-1):
271 Tectonophysics, v. 584, p. 23–42, doi:10.1016/j.tecto.2012.08.021.
272 Li, H., et al., 2015, Long-term temperature records following the M_w7.9 Wencuhan
273 (China) earthquake are consistent with low friction: Geology, v. 43, p. 163–166,
274 doi:10.1130/G35515.1.

Niemeijer, A.R., Di Toro, G., Nielsen, S., and Di Felice, F., 2011, Frictional melting of gabbro under extreme experimental conditions of normal stress, acceleration and sliding velocity: Journal of Geophysical Research, v. 116, B07404, doi:10.1029/2010JB008181.

Oohashi, K., Hirose, T., and Shimamoto, T., 2011, Shear-induced graphitization of carbonaceous materials during seismic fault motion: experiments and possible implications fault mechanics: Journal of Structural Geology, v. 33, p. 1122–1134, doi:10.1016/j.jsg.2011.01.007.

Oohashi, K., Hirose, T., Kobayashi, K., and Shimamoto, T., 2012, The occurrence of graphite-bearing fault rocks in the Atotsugawa fault system, Japan: Origins and implications for fault creep: Journal of Structural Geology, v. 38, p. 39–50, doi:10.1016/j.jsg.2011.10.011.

Pastewka, L., Moser, S., Gumbsch, P., and Moseler, M., 2011, Anisotropic mechanical amorphization drives wear in diamond: Nature Materials, v. 10, p. 34–38.

Ross, J.V., and Bustin, R.M., 1990, The role of strain energy in creep graphitization of anthracite: Nature, v. 343, p. 58–60, doi:10.1038/343058a0.

Rowe, C.D., and Griffith, W.A., 2015, Do faults preserve a record of seismic slip: A second opinion: Journal of Structural Geology, v. 78, p. 1–26, doi:10.1016/j.jsg.2015.06.006.

Rumble, D., 2014, Hydrothermal graphitic carbon: Elements, v. 10, p. 427–433, doi:10.2113/gselements.10.6.427.

296 Rutter, E.H., Hackston, A.J., Yeatman, E., Brodie, K.H., Mecklenburgh, J., and May,
297 S.E., 2013, Reduction of friction on geological faults by weak-phase smearing:
298 Journal of Structural Geology, v. 51, p. 52–60, doi:10.1016/j.jsg.2013.03.008.
299 Si, J., Li, H., Kuo, L.W., Pei, J., Song, S.R., and Wang, H., 2014, Clay mineral anomalies
300 in the Yingxiu–Beichuan fault zone from the WFSD-1 drilling core and its
301 implication for the faulting mechanism during the 2008Wenchuan earthquake (Mw
302 7.9): Tectonophysics, v. 619–620, p. 171–178, doi:10.1016/j.tecto.2013.09.022.
303 Sibson, R.H., and Toy, V.G., 2006, The habitat of fault-generated pseudotachylyte:
304 Presence vs. absence of friction-melt, *in* Abercrombie, R., et al., eds., Earthquakes:
305 Radiated Energy and the Physics of Faulting: Washington, D.C., American
306 Geophysical Union, p. 153–166, doi:10.1029/170GM16.
307 Sibson, R.H., 2003, Thickness of the seismic slip zone: Bulletin of the Seismological
308 Society of America, v. 93, p. 1169–1178, doi:10.1785/0120020061.
309 Smith, S.A.F., Di Toro, G., Kim, S., Ree, J.-H., Nielsen, S., Billi, A., and Spiess, R.,
310 2012, Coseismic recrystallization during shallow earthquake slip: Geology, v. 41,
311 p. 63–66, doi:10.1130/G33588.1.
312 Thomas, P., Delbe, K., Himmel, D., Mansot, J.L., Cadore, F., and Guerin, K., 2006,
313 Tribological properties of low-temperature graphite fluorides: Influence of the
314 structure on the lubricating performances: Journal of Physics and Chemistry of
315 Solids, v. 67, p. 1095–1099, doi:10.1016/j.jpcs.2006.01.084.
316 Wang, Y., Ma, S., Shimamoto, T., Yao, L., Chen, J., Yang, X., He, H., Dang, J., Hou, L.,
317 and Togo, T., 2014, Internal structures and high-velocity frictional properties of

Longmenshan fault zone at Shenxigou activated during the 2008 Wenchuan earthquake: Earth Science, v. 27, p. 499–528, doi:10.1007/s11589-014-0096-6.

Wang, H., Li, H., Janssen, C., and He, X., 2016, Seismic energy partitioning during the 2008 Mw 7.9 Wenchuan earthquake from WFSD-1 core sample: Abstract S33C–2850 presented at the 2016 Fall Meeting, American Geophysical Union, San Francisco, California, 12–16 December.

Xue, L., et al., 2013, Continuous permeability measurements record healing inside the Wenchuan earthquake fault zone: Science, v. 340, p. 1555–1559, doi:10.1126/science.1237237.

Yao, L., Ma, S., Platt, J.D., Niemeijer, A.R., and Shimamoto, T., 2015, The crucial role of temperature in high-velocity weakening of faults: Experiments on gouge using host blocks with different thermal conductivities: Geology, v. 44, p. 63–66, doi:10.1130/G37310.1.

FIGURE

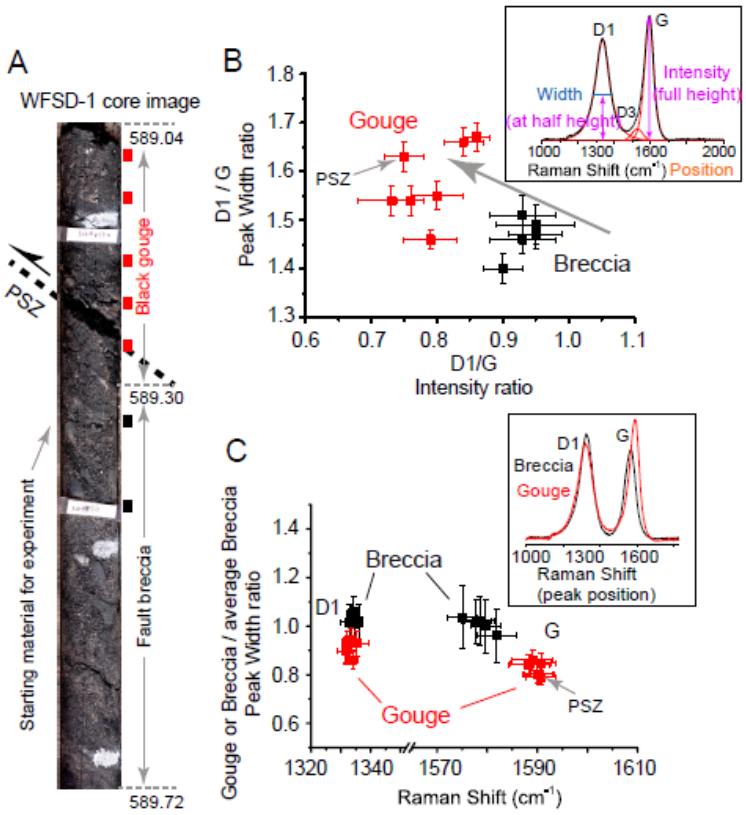

Figure 1. Wenchuan earthquake Fault Scientific Drilling WFSD-1 borehole core with location of the studied samples (southeast Tibet) and results of the micro-Raman analysis. A: Core images exhibiting major portions of the Longmenshan fault along the WFSD-1 borehole. Location of the analyzed samples are indicated by red (black gouge) and black (breccia) in color boxes. B: Defect band (D1) to graphite band (G) (D1/G) peak width ratio versus D1/G intensity ratio. The inset shows a representative first-order region of Raman spectrum and defines the relevant spectrum decomposition parameters (width, intensity, etc.). C: D1 or G peak width of gouge over average breccia peak width versus G band peak position. The inset shows the systematic shift toward higher frequencies of the G band observed in black gouge with respect to the fault breccia.

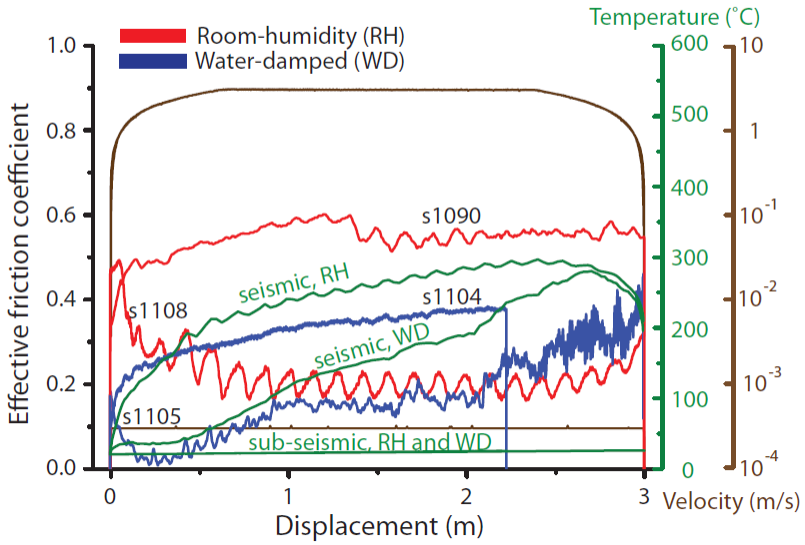

Figure 2. Experiments performed with the rotary machine SHIVA on carbonaceous materials (CMs)–bearing materials from the Longmenshan fault, southeast Tibet. The effective friction coefficient (shear stress / normal stress) versus displacement for four experiments (Item DR2 [see footnote 1]) performed at almost subseismic and seismic slip rates under room humidity (s1090 and s1108) and water-dampened (s1105 and s1104) conditions. The modeled temperature evolution with slip in the slipping zones obtained with COMSOL (https://www.comsol.com) multiphysics are shown for experiments s1090, s1104, s1105, and s1108 (green in color curves). The slip velocity curves for all experiments are shown in brown.

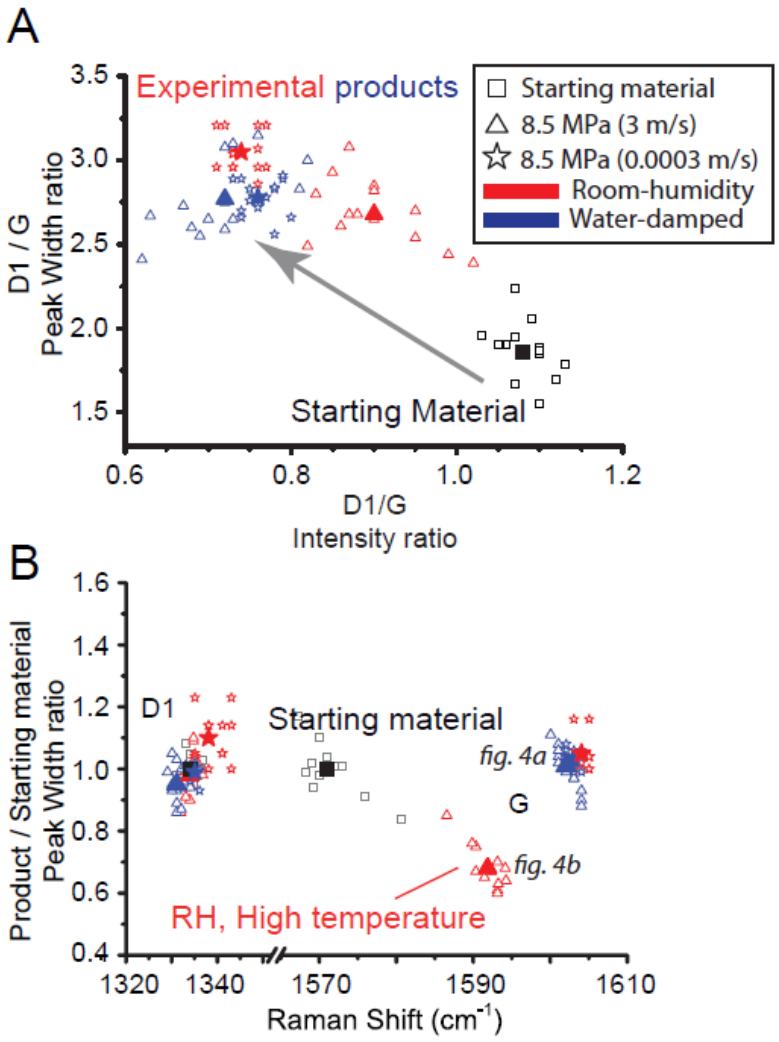

356

357 Figure 3. Raman spectra analysis of gouges sheared in rock friction experiments. A:

358 Defect band (D1) to graphite band (G) (D1/G) peak width ratio versus D1/G intensity

359 ratio. B: D1 or G peaks width of sheared gouges (normalized by the average starting

360 material peak widths) versus D1 or G band peak position. Two representative

361 experimental products were selected for microstructural analysis (see Fig. 4).

362

363

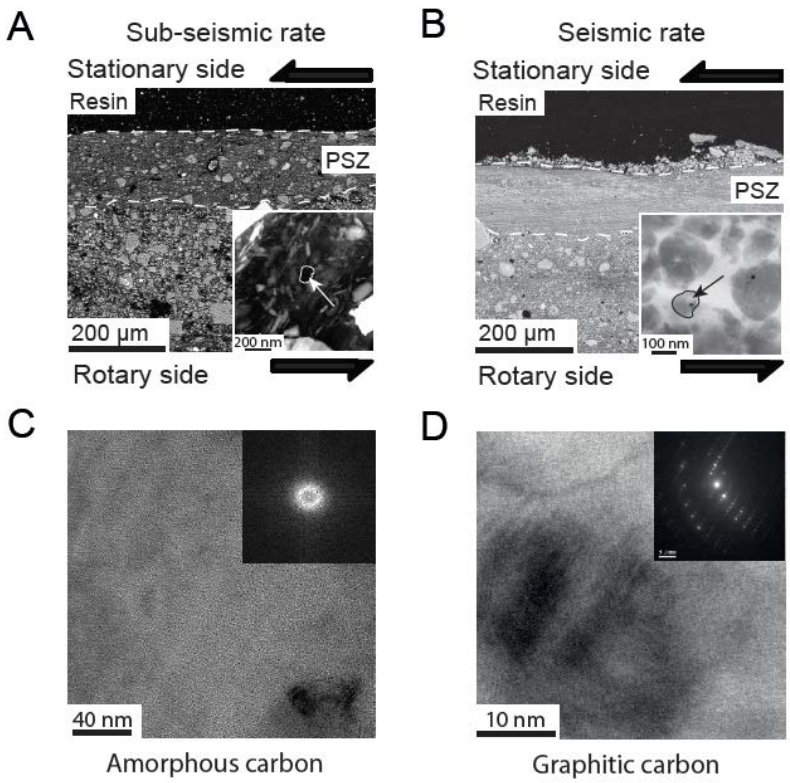

364

365 Figure 4. Microstructures in gouges sheared under room humidity conditions at almost
366 subseismic (experiment s1090) and seismic (experiment s1002) slip rates. A,B: Strain
367 localized in principal slip zones (PSZ). Inset shows the presence of carbonaceous
368 materials (CMs) within the PSZ (field-emission scanning electron microscopy images).
369 C: Poorly ordered carbon grains (see selected area electron diffraction [SAED] pattern in
370 inset) within the PSZ formed at subseismic slip rates (transmission electron microscopy
371 [TEM] image). : Well-crystallized carbon (see SAED pattern in the inset) within the PSZ
372 formed at seismic slip rates (TEM image).

373

[1]GSA Data Repository item 2017xxx, xxxxxxxx, is available online at http://www.geosociety.org/datarepository/2017/ or on request from editing@geosociety.org.